Development of Volume-Average Theory for Deep-Bed Filtration

E. A. Stephan and G. G. Chase
Dept. of Chemical Engineering, The University of Akron, Akron, OH 44325

Over the past 20 years, researchers have attempted, with limited success, to develop a general correlation for permeability loss within a deep-bed filter. The research presented here yields a unique result by rigorously developing a filtration model that focuses on the effective surface area as the dominant factor causing permeability loss. Both a constitutive relation and a geometric interpretation are developed to represent the effective surface area. The resulting macroscale equations accurately model the permeability reduction by incorporating the lower scale mechanisms. The model was tested using the specific process of water injection into a sandstone formation with experimental variables of salt concentration, pH, and concentration of influent fines. Postulated forms of the constitutive relations were verified through these experiments. By accounting for the changes in effective surface area, the model uniquely and accurately describes the permeability loss within a deep-bed filter.

Introduction

Currently, there is no widely accepted model for permeability loss during deep-bed filtration. The majority of the past mechanistic research efforts in deep-bed filtration have been limited to the micro- and molecular-scale level, with limited success in relating these quantities to the macroscale experimental observations. The work conducted at the microscopic level has greatly enhanced the understanding of the mechanisms behind deep-bed filtration. Due to their complexity, however, these models are limited to simple geometric representations, and most have not been verified experimentally. Macroscopic research has yielded experimental information concerning specific applications, with little investigation of the mechanisms behind the phenomena. Most of these models are heuristically developed and are not accepted as an accurate representation of a deep-bed filtration process.

The volume-average scale has largely been ignored and is the main focus of this work. Used for multiphase systems, the volume-average equations are analogous to the basic concepts for single-phase systems, but have ''excess terms'' to account for phase interaction (Willis et al., 1991). To model the macroscopic permeability loss, mechanisms are proposed at the volume-average scale. These mechanisms are developed using theories from the micro- and molecular scales. To translate between the scales, the operational approach, a formalization of the scientific method, is used. Figure 1 shows the methodology as applied to typical chemical processes.

To use the operational approach, the first step is determining the phenomena and appropriate scales of interest. Then, the lower scale mechanisms controlling the phenomena are postulated using the basic concepts. Theories and experiments at even lower scales aid in forming these postulates. Next, averaging the basic concepts yields a correlation for the phenomena.

The mean-value theorem for integrals is the basis for the averaging process (Willis et al., 1991). This theorem states that for a given function $f(x)$, a unique average value, $\langle f \rangle$, can be determined. Conversely, there may be an infinite number of functions that yield a given average value. Thus, it is possible for multiple sets of postulates to exist that explain the same phenomena. The higher scale correlation implicitly accounts for the details of the mechanism, hidden in the functional form of $f(x)$. Specifically, when working with porous media, this loss of information is of practical value, since it eliminates the need for experimental data that is often inaccurate or unattainable. As shown in Figure 2, the use

Correspondence concerning this article should be addressed to G. G. Chase.

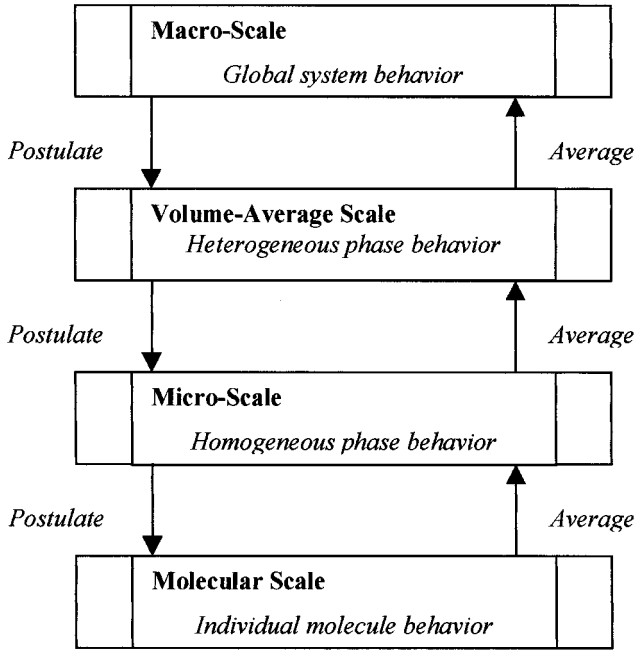

Figure 1. Methodology for translating model equations between scales.

Involves both the postulating of mechanisms and the averaging of the basic concepts to yield a correlation.

of averaging allows a model that is developed based on one type of porous medium to be applicable to many different media. In this work, the fundamental equations and constitutive relations for general deep-bed filtration are rigorously derived from the basic concepts. The one-dimensional flow equations are applied to the process of water injection through a sandstone formation. Core flood experiments are used to determine model parametric values.

Continuum Theory

Development of volume-averaged equations

A cylinder filled with a porous media, composed of a large number of small solid particles, is depicted on the left side of Figure 3. The surface area of the particles is much greater than the surface of the tube, such that under laminar flow conditions all of the fluid-phase momentum is transferred to the medium. This mechanism permits the equivalent representation shown on the right side of Figure 3, in which the solid particles form an "insulating" barrier to prevent the transfer of momentum to the tube walls. For this system, there are two phases: a fluid (denoted α) and a solid (β). Within each phase, there are three possible species: liquid (l), medium (m), and fine particles (f).

Assumptions

The general model was applied to the specific process of secondary oil recovery involving water injection into a sandstone formation. Deep-bed filtration during secondary oil recovery is a very dynamic, complex system. The following assumptions, coupled with the system description below, simplified the analysis.

- The fluid and the solid are consistent in temperature. Any additional fluid injected into the system is at the same temperature (Stephan, 1999).
- All flow is Newtonian, laminar, and unidirectional. The fluid is considered single phase, single species.
- The medium is incompressible, stationary, and oil-free.
- No chemical reaction occurs between any of the species.
- The medium and the particle densities are constant.
- The fine particle diameters are an order of magnitude smaller than the medium particle diameters.

The particles migrate between the fluid and the solid phase in the radial direction. If entrained in the fluid, the particles

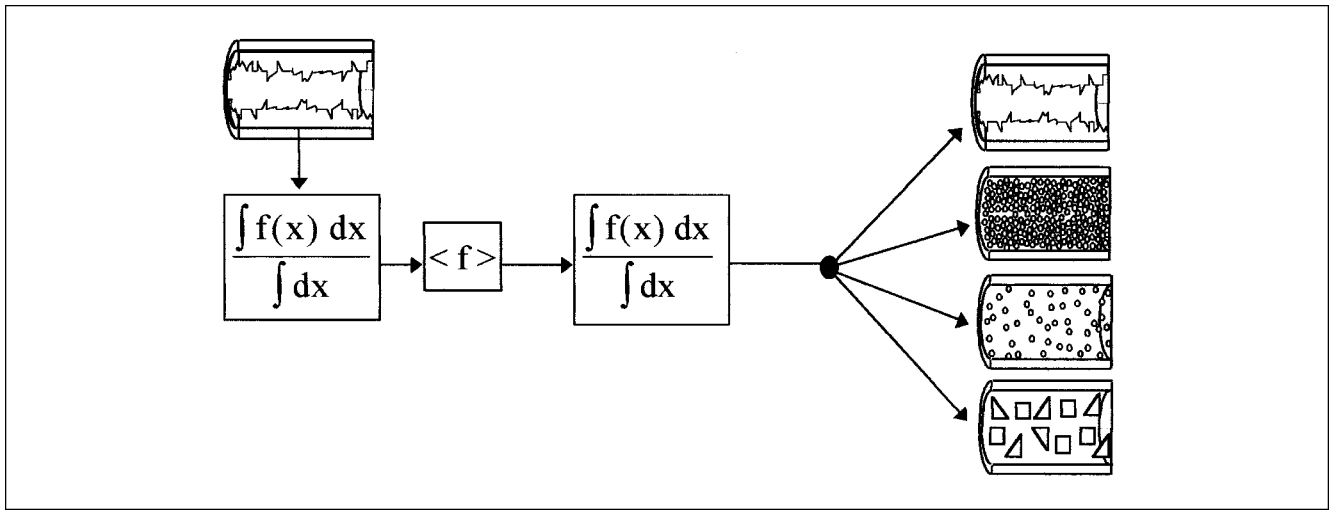

Figure 2. By using the mean-value theorem, a specific porous media model (left) can be applied to a wide range of media types (right).

It is done by averaging information that is often unattainable (Stephan et al., 1997).

move axially with a velocity equal to the fluid-phase velocity. Once the particles move into the solid phase, they become stationary. The flux term in the species balance accounts for the movement of particles between phases (Bird et al., 1960). The basic concepts required to model the system are the mass balance and the momentum balance. A conservation-of-mass equation can be written for each phase and each species within the phase. Of the six conservation-of-mass equations, only four are independent. The momentum balances for each phase are formed by conducting an order-of-magnitude study. The effects of accumulation, convection, and liquid stress terms are considered insignificant when compared to the drag force and solid matrix stress term, and are thus neglected (Chase and Willis, 1992).

The governing equations at the continuum scale for the system are spatially averaged over the cross section using the fundamental theorem of calculus and the mean-value theorem of integrals. This process yields the volume-average scale equations, which govern flow in porous media. The continuum scale notation applies to the ''insulating'' model of momentum transfer, while the resulting volume-average equations allow the model to apply to any porous media with a large surface area. The averaging process eliminates the need for information at the pore scale, which is often unattainable or inaccurate. All equations are summarized in Table 1.

Table 1. Basic Concepts for DBF Process

Mass Balances	
Species Balances	
$\frac{\partial \rho^{\ell\alpha}}{\partial t} = 0$	(1)
$\frac{\partial \rho^{f\alpha}}{\partial t} + \frac{1}{r}\frac{\partial}{\partial r}(r n_r^{f\alpha}) + \frac{\partial}{\partial z}(n_z^{f\alpha}) = 0$	(2)
$\frac{\partial \rho^{m\beta}}{\partial t} = 0$	(3)
$\frac{\partial \rho^{f\beta}}{\partial t} + \frac{1}{r}\frac{\partial}{\partial r}(r n_r^{f\beta}) = 0$	(4)
Microscopic Balances	
$\frac{\partial \rho^{\alpha\alpha}}{\partial t} + \frac{1}{r}\frac{\partial}{\partial r}(r n_r^{f\alpha}) + \frac{\partial}{\partial z}(n_z^{f\alpha}) = 0$	(5)
$\frac{\partial \rho^{f\beta}}{\partial t} + \frac{\partial \rho^{m\beta}}{\partial t} + \frac{1}{r}\frac{\partial}{\partial r}(r n_r^{f\beta}) = 0$	(6)
Volume-Averaged Balances	
$\frac{\partial}{\partial t}[\epsilon_\alpha \langle \rho^{\alpha\alpha} \rangle] + \frac{\partial}{\partial z}[\epsilon_\alpha \bar{v}_{\alpha,z} \langle \rho^{f\alpha} \rangle] + a_\beta n_{R(z)}^{f\alpha} = 0$	(7)
$\frac{\partial}{\partial t}[\epsilon_\beta \langle \rho^{\beta\beta} \rangle] - a_\beta n_{R(z)}^{f\beta} = 0$	(8)
Momentum Balances	
Microscopic Balances	
$\frac{1}{r}\frac{\partial}{\partial r}(r\tau_{rz}^{\alpha}) + \frac{\partial P^{\alpha}}{\partial z} = 0$	(9)
$\frac{1}{r}\frac{\partial}{\partial r}(r\tau_{rz}^{\beta}) + \frac{\partial \tau_{zz}^{\beta}}{\partial z} + \frac{\partial P^{\alpha}}{\partial z} = 0$	(10)
Volume Average Balances	
$a_\beta \tau_{rz}^{\alpha}\vert_{R(z)} + \frac{d}{dz}(\epsilon_\alpha P^{\alpha}) = 0$	(11)
$-a_\beta \tau_{rz}^{\beta}\vert_{R(z)} + \frac{d}{dz}(\epsilon_\beta \langle \tau_{zz}^{\beta\beta} \rangle) + \frac{d}{dz}(\epsilon_\beta P^{\alpha}) = 0$	(12)
Constitutive Relations	
$a_\beta n = \lambda \rho_\alpha \omega^{f\alpha} - \kappa \rho_\beta (\omega^{f\beta} - \bar{\omega}^{f\beta})$	(13)
$a_\beta = Y_m \sigma(4\pi R_m^2) + Y_f(\sigma(4\pi R_f^2) - A_\Delta)$	(14)
$A_\Delta = \frac{1}{2}R_m^2\left[2\sin^{-1}\left(1.73\frac{R_f}{R_m}\right) - \sin\left(2\sin^{-1}\left(1.73\frac{R_f}{R_m}\right)\right)\right]$	(15)
$\epsilon_\beta = \frac{\rho_m}{\rho^{mm}\Phi^{m\beta}}$	(16)
Process Correlations	
$k = \frac{Q\mu_\alpha L_{\text{bed}}}{A_{\text{bed}}\Delta P g_c}$	(17)
$\Delta P = \frac{BLQ\mu_\alpha a_\beta^2}{g_c \epsilon_\alpha^3 A}$	(18)
$\therefore k = \frac{\epsilon_\alpha^3}{Ba_\beta^2}$	(19)

Process correlations

Darcy's law and the Blake-Kozeny equation express the permeability and pressure drop, respectively, of a porous medium in terms of experimental, measurable quantities (Bird et al., 1960; ASTM D-4520-86). By inserting the particle diameter and superficial velocity definitions used in the development of the Blake-Kozeny equation, in combination with Darcy's law, the permeability can be found by the equation (Bird et al., 1960; McCabe et al., 1985; Stephan et al., 1997).

$$k = \frac{\epsilon_\alpha^3}{Ba_\beta^2}. \tag{19}$$

This correlation indicates that to theoretically predict the permeability [k], constitutive relations for the fluid-phase porosity [ϵ_α] and effective surface area [a_β] are required. The porosity and surface area change simultaneously, requiring a complex system of equations. The parameter B in this expression is the Blake-Kozeny constant. This is commonly set at 150/36, or 4.167. This value, however, evolved from an attempt to theoretically interpret Ergun's experimental data. Recent work by Fand et al. examined data collected over the past 50 years for porous media flow and concluded that a better fit is obtained by using a value of 5.35 ± 0.23 (Fand et al., 1987). Experiments conducted by Desai further support this finding (Desai, 1989). In his work, the permeability was measured during flow through wire mesh screens, chosen since the porosity and surface area could be accurately calculated. Analysis of his data yields a value of 5.25 over a range of laminar flow conditions. Therefore, this work uses a constant B value of 5.35.

Constitutive relations

Porosity. The porosity model utilizes the definitions of the particle volume fraction, grain density, and species bulk mass density, given, respectively, below (Stephan, 1999). In general, chemical species are not considered to be large enough to occupy a significant volume. In this work, however, it is desired to track the movement of the particles and their ef-

fect on the surface area. To accomplish this, the particles are considered large enough to have a volume assigned.

$$\Phi^{ij} \equiv \frac{V_i}{V_j} = \text{volume fraction of species } i \text{ in phase } j \quad (20)$$

$$\rho^{ii} \equiv \frac{M_{1i}}{V_{1i}} = \text{grain density of species } i \quad (21)$$

$$\rho_i = \sum_j \epsilon_j \Phi^{ij} \rho^{ii} = \sum_j \frac{M_i}{V_{\text{bed}}} = \text{bulk density}. \quad (22)$$

Rearranging these definitions as applied to the media yields the following relation for porosity:

$$\epsilon_\beta = \frac{\rho_m}{\rho^{mm} \Phi^{m\beta}} = \text{beta phase volume fraction}. \quad (16)$$

Effective Surface Area: Geometric Interpretation. The effective surface area for the total volume is the summation of the surface area of the medium and the surface area of the fines. Past research has calculated each individual surface area using the relation of porosity, equivalent spherical particle diameter [d_g], and sphericity [ϕ] (Bird et al., 1960; McCabe et al., 1985).

$$a_\beta = \frac{6}{\phi d_g}(1 - \epsilon_\alpha). \quad (23)$$

With both the sphericity and particle diameter constant, the surface area will change only with a change in porosity. A large number of particles must deposit or release to significantly alter the porosity, whose range by definition is limited between 0 and 1. Work by Donaldson supports this conclusion, demonstrating that while the permeability of a sandstone formation declined by two orders of magnitude during filtration experiments, the porosity changed by only 0.3% (Donaldson et al., 1977). Therefore, the most important parameter in the permeability equation is the effective surface area, and it requires a more accurate model than the commonly accepted equation.

A model for the effective surface area must account for two phenomena. The deposition of a particle onto a media particle, or ''collector,'' causes an increase in the surface area by addition of the area of the particle exposed to the streamline flow. However, it also causes a loss of area on the collector, due to a ''shadow effect'' (Tien and Payatakes, 1979). Once a collector captures a particle, a certain amount of area behind the particle is no longer available for deposition due to the alteration of the streamline flow pattern. To include both mechanisms in the surface area expression, a geometric representation of the surface-area change was developed, as shown in Figure 4.

The total effective surface area can be expressed as the summation of the number of particles [Y_i] multiplied by the surface area available for deposition on each particle, given in Eq. 14. The first term reflects the area of the medium and the second the area of the fine particles that is available for particle interception. Not all of the original media collector or the deposited particle is available for momentum transfer due to packing structure, fracturing, or cul-de-sac formations. The geometric parameter σ has been included to account for this loss of area. Furthermore, research by Liu demonstrated that non-Brownian-size particles are restricted to collision with the upper hemisphere of a collector due to interception effects (Liu et al., 1995). This places an upper bound of approximately 0.5 on σ:

$$a_\beta = Y_m \sigma \left(4\pi R_m^2\right) + Y_f \left(\sigma \left(4\pi R_f^2\right) - A_\Delta\right). \quad (14)$$

To account for the loss of collector area due to the shadow effect, A_Δ is derived as follows. A segment of a circle with the same diameter as the deposited particle approximates the amount of collector area lost (Spiegel, 1995). Substituting this information yields the following equation for the lost area. Since the amount of area lost must be positive, the lower bound of σ is dependent upon the size of the particles used:

$$A_\Delta = \frac{1}{2} R_m^2 \left[2\sin^{-1}\left(1.73\frac{R_f}{R_m}\right) - \sin\left(2\sin^{-1}\left(1.73\frac{R_f}{R_m}\right)\right)\right]. \quad (15)$$

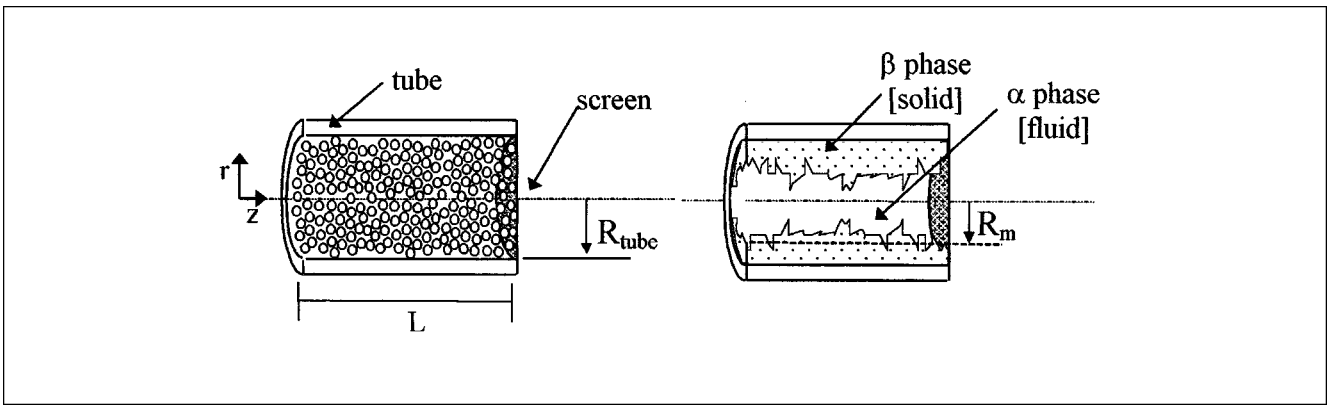

Figure 3. Model representation of high surface area porous medium (Stephan et al., 1997).

While this methodology yields the changes in surface area due to the deposition or release of particles, it fails to address the mechanisms that cause the change. The surface area is affected by the parameters of flow rate, salt concentration, pH, and the mass fraction of particles (Vaidya and Fogler, 1990). To obtain an expression for how these parameters alter the permeability, the flux expression must be examined.

Effective Surface Area: Theoretical Analysis. Coupling occurs between the effective surface area and the particle flux, n. Dimensional analysis of the solid-phase mass balance, Eq. 8, yields a function dependent upon the amount of fines present in each phase and a function of time, h. The resulting expression contains a migration flux analogous to the heat-transfer flux given by Newton's Law of Cooling (Bird et al., 1960):

$$a_\beta n[\,=\,]\frac{M_f}{t^* V_{\text{bed}}}[\,=\,]\frac{1}{t}\frac{M_f}{M_j}\frac{M_j}{V_{\text{bed}}} = f\left(:h, \omega^{fj}, \rho_j\right). \quad (24)$$

Based on this analysis and past research, the proposed form of the flux expression is equal to the amount of captured particles minus the amount of released particles (Khilar and Fogler, 1983; McDowell-Boyer et al., 1986; Baghdikian et al., 1989; Vaidya and Fogler, 1990).

$$a_\beta n = \lambda \rho_\alpha \omega^{f\alpha} - \kappa \rho_\beta \left(\omega^{f\beta} - \overline{\omega}^{f\beta}\right) \quad (13)$$

This equation introduces three new unknowns. Both κ, the release coefficient, and λ, the capture coefficient, have units of time and are functions of the water chemistry (Khilar and Fogler, 1983; McDowell-Boyer et al., 1986). Inclusion of $\overline{\omega}^{f\beta}$, the amount of fines that will not migrate, accounts for the fact that not all the fines present within a natural media are able to release due to physical limitations.

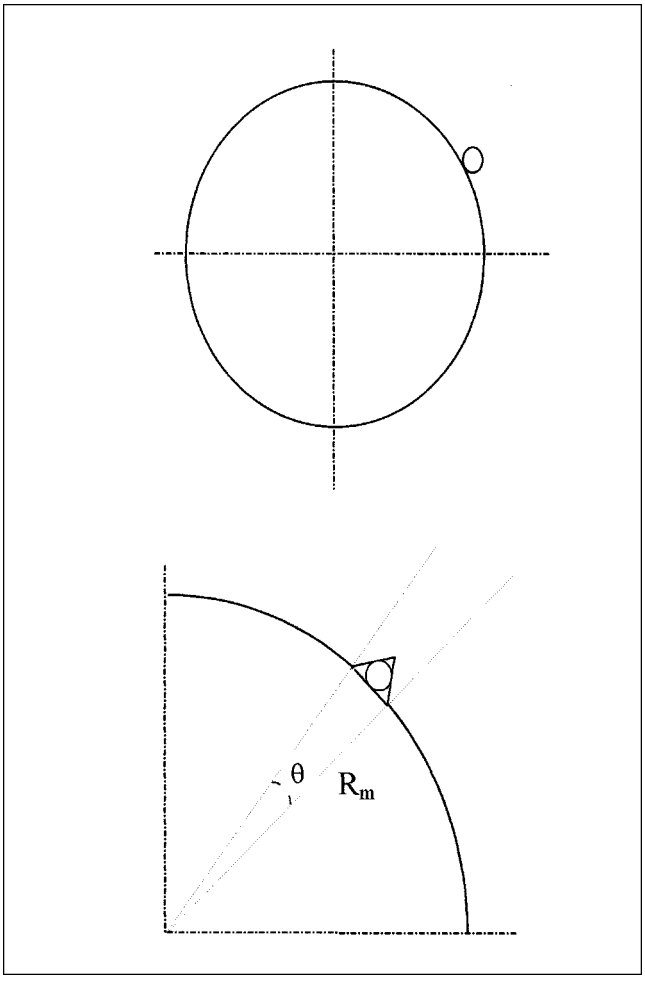

Figure 4. Geometric representation of particle deposition onto a media collector.

Solution procedure

To validate the proposed constitutive equations, a set of experiments must be conducted to determine the parametric values and evaluate the model accuracy. For this work, the model was evaluated using experiments constructed to simulate a secondary oil recovery operation. The validation process is summarized in Figure 5. During experimentation, the pressure drop and flow rate are monitored over time. The fluid viscosity and media dimensions are also measured. The permeability loss is determined from Darcy's law. Using the initial permeability and porosity, the surface area parameter is determined.

The effective surface area and porosity profiles can be calculated from the derived series of equations and definition utilizing the experimental permeability loss data. The use of an optimization program allows for the simultaneous solution of these equations by variation in the model parameters. A brief description of the optimization process is given elsewhere (Stephan, 1999). If the constitutive equations are validated by low model-to-data error values, the model is considered to be accurate.

Experimental Studies

Materials

Berea sandstone is the most commonly used reference sandstone in the petroleum industry. It contains 8% by weight of migrating-type clay, with no swelling-type clay (Khilar and Fogler, 1983). All samples were purchased from American Stone, Bernea, OH. The cores were cut from the formation to the specifications of 1.5-in. (38-mm) diameter by 2-in. (51-mm) length. The average sand diameter as measured on a microscope using Jandel image-analysis software was determined to be 30 μm. Therefore, for the model, the diameter of the media was set at 0.003 cm. The grain density of the sand was experimentally determined to be 2.67 g/cm^3 and the dry bulk density of the sand was determined to be 2.254 g/cm^3. The average core porosity was 16.3%.

Approximately 88% of the clay present in Berea sandstone is kaolinite clay (Khilar et al., 1983). To limit the scope of this research, the clay minerals within the formation will be considered to consist of pure kaolinite clay. Kaolinite is one of four types of clays that compose the kaolin class of clays. The chemical formula is $Al_2Si_2O_{10}(OH)_8$, with a typical grain density of 2.594 g/cm^3 (Carmichael, 1989). Kaolinite clay is platelet in shape (Moore, 1960).

To allow distinction between the indigenous and injected clay in the core studies, another clay was desired that exhibited similar properties to kaolinite and yet was measurably different. Based on zeta potential testing, the details of which are presented elsewhere, illite clay was chosen to represent the injected particles (Stephan, 1999). The Thiele Kaolin Company in Sandersville, GA, donated the kaolinite clay. The illite clay, sample No. 35 Fithian, IL, was purchased from Wards Natural Scientific Establishment.

The grain density of the kaolinite clay was determined to be 2.43 ± 0.085 g/cm^3. The size measurements for the clay were taken with the Hiac/Royco particle counter. The average particle size of the clay collected from the sand was 5.6 μm. The average size of the injected clay was 1.45 μm. Therefore, for the model, the diameter of the particle was set at 0.0003 cm.

Experimental design

To ascertain the necessary material parameters for the particle flux expression, a series of water injection experiments were conducted. An experimental design that could

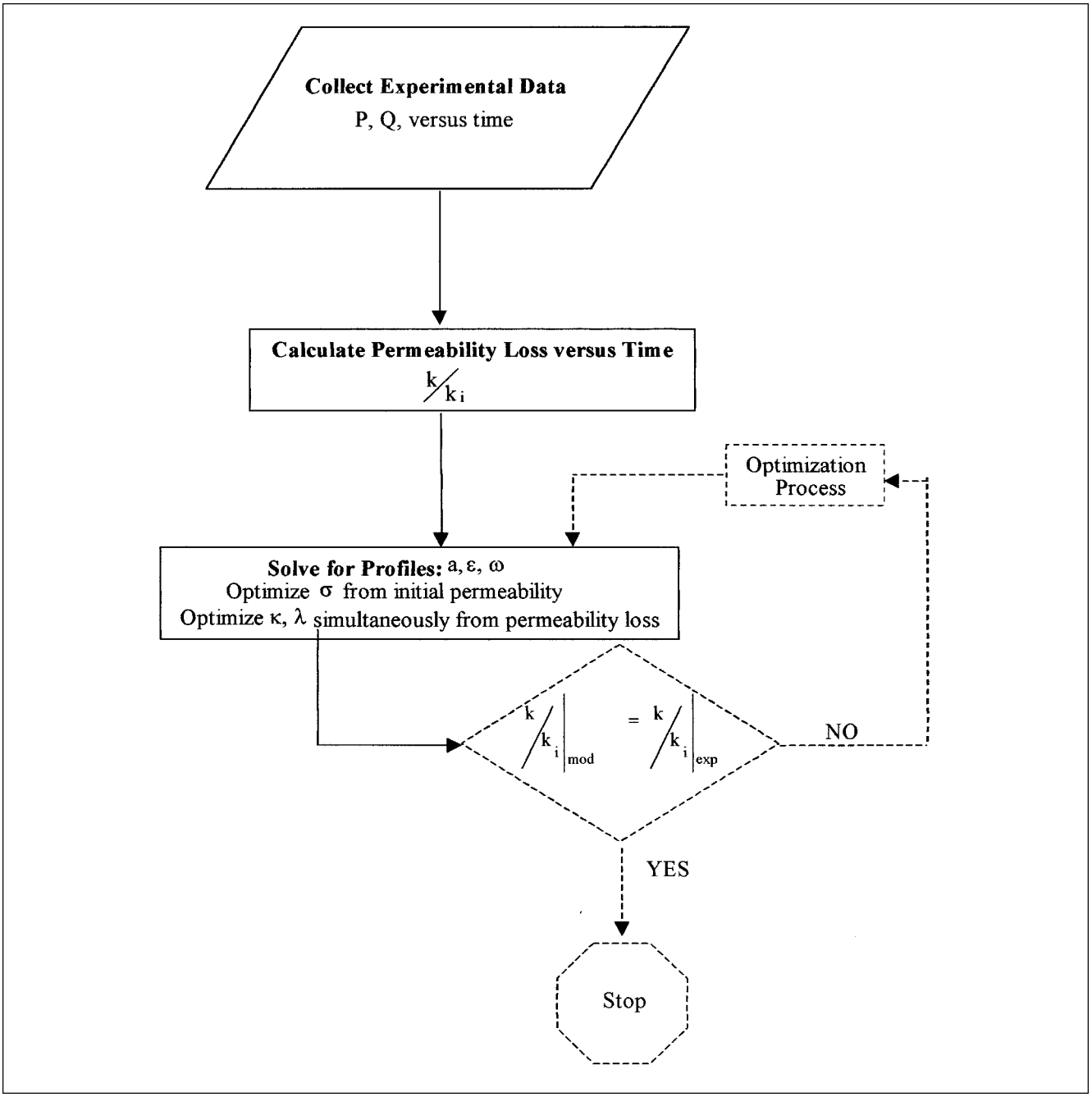

Figure 5. Calculation procedure.

handle a second-order model was desired, due to the flexibility and ease of parameter estimation provided by this level of design. The most common second-order design is a central composite design (CCD). The CCD is composed of a two-level factorial with axial points and center runs. The axial distance values for the variables, or their location from the center point, vary from 1 to $\sqrt{\gamma}$, where γ is the number of variables. In this work, a face-centered cubic (FCC) experimental design was utilized. A FCC is a CCD with the axial distance set to one, used when physical limitations prevent experimentation outside of the defined variable region (Myers and Montgomery, 1995). The pH is limited within the range of 0 to 14, thus making this design applicable. The variable levels in terms of physical measurements used were:

- Salt concentration (SC): 0 M, 0.07 M, and 0.14 M (Khilar and Fogler, 1984; Baghdikian et al., 1989; Vaidya and Fogler, 1992)
- pH: 4, 7, and 10 (Baghdikian et al., 1989; Vaidya and Fogler, 1990)
- Concentration of injected particles (IP): 0, 15, and 30 mg/L (Fram, 1994).

A resolution V was utilized for the factorial portion, such that no main effects or two-factor interactions were aliased with any other main effect or two-factor interaction. The experimental set conducted with no injection particles yielded information on the release coefficient. The capture coefficient was determined from experiments conducted at conditions of pH 4 and a salt concentration 0.14 M. Two center runs yielded the experimental error. It has been shown that the FCC is insensitive to the number of center runs used, and no further improvement in the variance estimation is observed with additional runs (Myers and Montgomery, 1995). The final experiments determined the effect of varying the injection concentration.

The cores were initially flooded with 0.5 M, pH 3 solution to obtain a base-line permeability. These conditions have been shown in previous research to not alter kaolin zeta potentials, allowing the clay to remain in a state of capture (Chang and Vigneswaran, 1990). This allows the measurement of the pressure drop through the core due to the drag force on the particles, and subsequent calculation of the effective surface area of the initial sand and clay matrix. These data were used to determine the surface-area parameter.

Equipment and procedures

The ASTM procedure D 4520-86, ''Standard Procedure for Determining Water Injectivity Through the Use of On-Site Floods'' (1986) composed the basis for the procedure. Initially, each sample was placed in polyolefin tubing to prevent channeling, and then glued into schedule 40 PVC to form a core holder. The holder was placed in two Plexiglas end-caps, sealed with O-rings, and tightened with four stabilization rods. This was then connected to the system piping through couplings. A 2-ft (0.6-m) section of 2-in. (51-mm) Schedule 80 PVC was used as a reservoir. Air pressure provided the driving force for the fluid, allowing both a constant pressure head and no temperature rise in the fluid due to viscous dissipation. Pressure measurements were taken macroscopically before and after the core holder with Rosemont 1151 SMART pressure cells (Eastman Kodak Company). The 1/8-in. pressure taps were drilled into the Plexiglas end-caps.

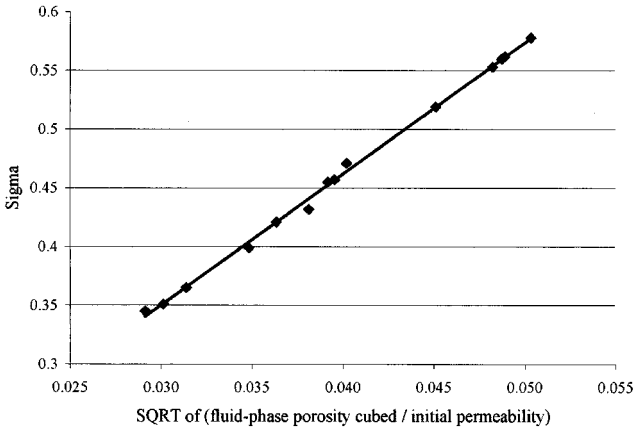

Figure 6. Surface-area parameter for media used in core-flood experiments.

Results and Discussion

Surface-area parameter

The surface-area parameter, σ, represents the percentage of a single-particle surface area available for momentum transfer. The results are shown in Figure 6, with the sigma value plotted against a function of porosity and permeability by way of Eq. 23. The original upper bound of 0.5 was found to be too restrictive for solution, and the model was allowed to vary between 0.027 and 1. The initial permeability experimental data matched with the program results with greater than 99.5% accuracy. According to the simulation results, approximately 35–55% of the surface area is available for momentum transfer and thus for particle capture. These values are in good agreement with previous research, which indicated that particle collisions were limited to the upper hemisphere of a collector (Liu et al., 1995).

Release and capture coefficients

The results of the core flood experiments are shown graphically in Figures 7 and 8. The results of the coefficients and the least-squares (L-S) error determined in matching the permeability loss are listed in Table 2.

High Salt Concentration Conditions. The model results for the conditions of high SC are shown in Figure 7. The release coefficient is approximately constant over the change in pH during the experiments where no particles were present in the injection water. The introduction of illite particles into the media caused an order-of-magnitude increase in the kappa value. This indicates that there must be an increase in the amount of particles released during the initial pore volumes to obtain the curve shape. This result demonstrates that there may be clay particle interactions occurring, causing the release of kaolinite particles due to intermolecular interactions.

Low Salt Concentration Conditions. The model results for the conditions of low SC are shown in Figure 8. The coefficients remain approximately constant at low pH. Since the system is already at a level of maximum permeability loss, the

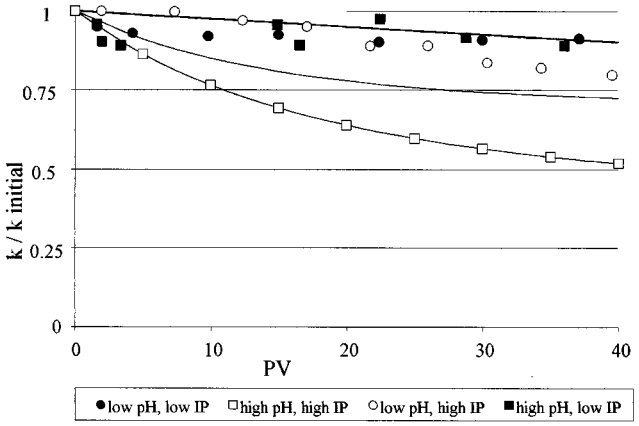

Figure 7. Permeability loss vs. PV for conditions of high salt concentration.

IP = injected particle concentration.

addition of illite particles has little effect under these conditions.

Under the conditions of high pH, however, the addition of illite particles has a drastic effect. The κ and λ values both increase by over an order of magnitude. These results further validate the proposed mechanism of clay particle interaction.

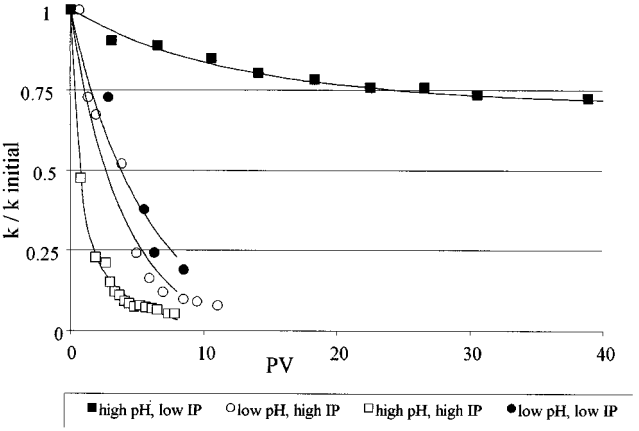

Figure 8. Permeability loss vs. PV for conditions of low salt concentration.

IP = injected particle concentration.

Model Benefits and Limitations. The model matched the experimental data within a 3% error, except for the run conducted under conditions of low SC, high pH, and high injected particle concentration. The model was unable to accurately duplicate the extreme drop in permeability observed during the first few pore volumes in this instance and returned an error of 7.5%. In addition, the model was unable to handle data below a 95% loss of permeability. Since any loss greater than 90% is irrelevant in filtration operation, this is not seen as a hindrance to the model. Two duplicate runs were conducted to calculate the effect of experimental error on the repeatability of the system. These runs gave a variation of 2% in the permeability loss data, well within the limits of the maximum experimental error.

Conclusions

Previous attempts to model the permeability loss during deep-bed filtration have had limited success. These models approximated the surface area in terms of porosity, particle diameter, and sphericity. The error introduced by these approximations is the primary factor inhibiting model accuracy. The most essential parameter in determining permeability, the effective surface area, has been largely neglected in past research. Through a unique development utilizing the operational approach and the basic concepts, a model was developed to account for the change in effective surface area during deep-bed filtration. By treating the movement of particles as a flux, an expression was developed to model the capture and release of particles within the media. The model equations were combined with a genetic algorithm optimization program, allowing sample parameters to be determined from minimal experimentation on sandstone media and clay particles. The results describe the permeability loss under a variety of water chemistry conditions to 97% accuracy for permeability loss up to 90%.

For future work, more experimental runs should be conducted with the flow rate and porosity monitored more accurately. This will help quantify the amount of permeability loss due to viscous drag on the fines. The concentration of fines introduced in the injection water should also be examined more extensively. Specifically, the concentration and the size distribution of fines introduced should be jointly tested. The size distribution may prove to be as significant a factor in the permeability loss observed during water injection operations

Table 2. Parametric Results for Kappa, Lambda Determination

SC	pH	IP	k Loss	Kappa	Lambda	LS Error (%)
High	Low	Low	10% in 40 PV	1×10^{-4}	2×10^{-5}	0.03
		High	25% in 40 PV	8.4×10^{-4}	1.8×10^{-2}	2.84
	High	Low	10% in 40 PV	1×10^{-4}	3×10^{-5}	0.02
		High	55% in 40 PV	1.3×10^{-3}	1.4×10^{-2}	0.57
Low	Low	Low	99% in 20 PV	6.7×10^{-3}	2.7×10^{-2}	0.31
		High	99% in 15 PV	9.9×10^{-3}	4.4×10^{-2}	1
	High	Low	30% in 40 PV	9.5×10^{-4}	2×10^{-2}	0.47
		High	99% in 10 PV	3.6×10^{-2}	2.6×10^{-1}	7.5
Neutral	Neutral	Low	20% in 60 PV	1.3×10^{-3}	3.5×10^{-2}	1.08
		High	32% in 60 PV	1.6×10^{-2}	3.2×10^{-2}	1.45%

Notation: SC = salt concentration; IP = injected particle concentration; k = permeability; LS Error = least squares error.

as the filtration size. This should be considered as a parameter worth monitoring and controlling.

Acknowledgments

The authors thank the following organizations for their financial contributions: The University of Akron, College of Engineering; NSF Grant CTS 9523524; Consortium for Development and Commercialization of Fine Particle Technologies, Ohio Board of Regents; and The Produced Water Conference, 1995–1999.

Notation

A_{bed} = area of porous media, cm^2
g_c = gravitational constant, = 32.174 lb·in./lbf·sec
L = height of porous media, cm
M_i = mass of species I,
P = pressure, Pa
Q = flow rate, cm^3/s
r = radial coordinate measurement, cm
R_g = radius of object g, cm
t = time measurement, s
V_{bed} = volume of bed, cm^3
z = axial coordinate measurement, cm
μ_α = intrinsic fluid-phase viscosity, g/cm·s
v^j = velocity of phase j, cm/s
v_0 = fluid-phase superficial velocity, cm/sec
ρ^{ij} = mass concentration of species i in phase j, g/cc
ρ^{jj} = phase average density, g/cc
ρ_j = phase j bulk density, g/cc
ω^{ij} = mass fraction of species i in phase j
θ = cylindrical coordinate measurement, rad

Literature Cited

ASTM Standard D 4520-86: "Standard Practice for Determining Water Injectivity Through the Use of On-Site Floods," American Society for Testing and Materials, Philadelphia, 1986.

Baghdikian, S. Y., M. M. Sharma, and L. L. Handy, "Flow of Clay Suspensions Through Porous Media," *SPE Reservoir Eng.*, **4**, 213 (1989).

Bird, R. B., W. E. Steward, and E. N. Lightfoot, *Transport Phenomena*, Wiley, New York (1960).

Carmichael, R. S., ed., *Practical Handbook of Physical Properties of Rocks and Minerals*, CRC Press, Boca Raton, FL (1989).

Chang, J. S., and S. Vigneswaran, "Ionic Strength in Deep Bed Filtration," *Water Res.*, **24**, 1425 (1990).

Chase, G. G., and M. S. Willis, "Compressive Cake Filtration," *Chem. Eng. Sci.*, **47**, 1373 (1992).

Desai, F. N., "Balance Equations and Constitutive Equations for Porous Media Flows with Large Porosity Gradients," PhD Diss., The Univ. of Akron, Akron, OH (1989).

Donaldson, E. C., B. A. Baker, and H. B. Carroll, "Particle Transport in Sandstones," 1977 SPE Annual Technical Conference and Exhibition, Denver, CO (1977).

Fand, R. M., B. Y. Kim, A. C. C. Lam, and R. T. Phan, "Resistance to the Flow of Fluids Through Simple and Complex Porous Media Whose Matrices are Composed of Randomly Packed Spheres," *J. Fluids Eng.*, **109**, 268 (1987).

Fram, J. W., "Well Kill Study of Thermal Producers in the South Belridge Field, CA," *SPE Prod. Facil.*, **9**, 165 (1994).

Khilar, K. C., and H. S. Fogler, "Water Sensitivity of Sandstones," *Soc. Petrol. Eng. J.*, **23**(1), 55 (1983).

Khilar, K. C., and H. S. Fogler, "The Existence of a Critical Salt Concentration for Particle Release," *J. Colloid Inter. Sci.*, **101**, 214 (1984).

Khilar, K. C., H. S. Fogler, and J. S. Ahluwalia, "Sandstone Water Sensitivity: Existence of a Critical Rate of Salinity Decrease for Particle Capture," *Chem. Eng. Sci.*, **38**, 789 (1983).

Liu, D., P. R. Johnson, and M. Elimelech, "Colloid Deposition Dynamics in Flow Through Porous Media," *Environ. Sci. Technol.*, **29**, 2963 (1995).

McCabe, W. L., J. C. Smith, and P. Harriott, *Unit Operations for Chemical Engineers*, McGraw-Hill, New York (1985).

McDowell-Boyer, L. M., J. R. Hunt, and N. Sitar, "Particle Transport through Porous Media," *Water Resour. Res.*, **22**, 1901 (1986).

Moore, J. W., "An Analysis of Clay Minerology Problems in Oil Recovery: I," *Pet. Eng.*, **32**, 40 (1960).

Myers, R. H., and D. C. Montgomery, *Response Surface Methodology: Process & Product Optimization Using Designed Experiments*, Wiley, New York (1995).

Spiegel, M. R., *Mathematical Handbook*, Schaum's Outline Series, McGraw-Hill, New York (1995).

Stephan, E. A., *Examination of Deep Bed Filtration*, PhD Diss., The Univ. of Akron, Akron, OH (1999).

Stephan, E. A., M. S. Willis, R. Vengimalla, and V. K. N. Yerra, "A Modern Development of Friction Factors in Porous Media," *AIChE Symposium Series — Fluidization/Fluid-Particle Systems*, AIChE, New York (1997).

Tien, C., and A. C. Payatakes, "Advances in Deep Bed Filtration," *AIChE J.*, **25**, 737 (1979).

Vaidya, R. N., and H. S. Fogler, "Fines Migration and Formation Damage: Influence of pH and Ion Exchange," *SPE Production Eng.*, **4**, 325 (1992).

Vaidya, R. N., and H. S. Fogler, "Formation Damage Due to Colloidally Induced Fines Migration," *Colloids Surf.*, **50**, 215 (1990).

Willis, M. S., I. Tosun, W. Choo, G. G. Chase, and F. Desai, "A Dispersed Multiphase Theory and its Application to Filtration," *Advances in Porous Media*, Elsevier, Amsterdam (1991).

Manuscript received Aug. 13, 1999, and revision received Apr. 21, 2000.